On the effects of liquid-gas interfacial shear on slip flow through a parallel-plate channel with superhydrophobic grooved walls

Chiu-On Ng,[1,a)] Henry C. W. Chu,[1] and C. Y. Wang[2]
[1]*Department of Mechanical Engineering, The University of Hong Kong, Pokfulam Road, Hong Kong*
[2]*Department of Mathematics, Michigan State University, East Lansing, Michigan 48824, USA*

(Received 26 April 2010; accepted 7 September 2010; published online 28 October 2010)

Comparisons between slip lengths predicted by a liquid-gas coupled model and that by an idealized zero-gas-shear model are presented in this paper. The problem under consideration is pressure-driven flow of a liquid through a plane channel bounded by two superhydrophobic walls which are patterned with longitudinal or transverse gas-filled grooves. Effective slip arises from lubrication on the liquid-gas interface and intrinsic slippage on the solid phase of the wall. In the mathematical models, the velocities are analytically expressed in terms of eigenfunction series expansions, where the unknown coefficients are determined by the matching of velocities and shear stresses on the liquid-gas interface. Results are generated to show the effects due to small but finite gas viscosity on the effective slip lengths as functions of the channel height, the depth of grooves, the gas area fraction of the wall, and intrinsic slippage of the solid phase. Conditions under which even a gas/liquid viscosity ratio as small as 0.01 may have appreciable effects on the slip lengths are discussed. © *2010 American Institute of Physics*. [doi:10.1063/1.3493641]

I. INTRODUCTION

Much knowledge has been garnered in the past decade on the mechanics of slip flow past a superhydrophobic surface. Velocity slip is an apparent phenomenon, arising from a composite boundary condition on the microscale. Surface roughness, microbubbles, hydrophobicity, and a low-density depletion region are the key qualities that make up a superhydrophobic surface. Slip leads to drag reduction and is important in microchannel flows. The body of work in this area has been fast growing in recent years. Reviews by Neto *et al.*,[1] Lauga *et al.*,[2] Zhang *et al.*,[3] and Rothstein[4] and the references therein can be consulted for the state of the art, in terms of experimental observations, mathematical modeling, and numerical simulations of slip on superhydrophobic surfaces.

A superhydrophobic surface is often a surface with fabricated microfeatures, such as ribs, posts, or holes. When the material is hydrophobic (i.e., with a contact angle larger than 90°) and the liquid pressure is below the capillary pressure, the liquid is restricted to the top of the microprotrusions, and the voids in the microfeature are occupied by a gas phase. In this Cassie state, the liquid flow is lubricated by the underlying gas. In addition, intrinsic slippage on a solid surface may result from a liquid depletion layer if the surface is coated with a hydrophobic chemical. The combination of lubrication over gas pockets and intrinsic slippage over solid phase accounts for the superhydrophobicity of a surface.

Surface slip is measured by the slip length,[5] which is defined as the depth into the envelope of a surface where the velocity would extrapolate to zero. Slip length is also equal in magnitude to the slip velocity per unit shear rate of flow near a boundary surface.

In mathematical modeling of the flow described above, it is often assumed for simplicity that the liquid-gas interface is flat and shear-free (e.g., Teo and Khoo).[6] On proposing some scaling laws, Ybert *et al.*[7] looked into the finite viscous dissipation in the gas phase and the meniscus curvature effects. Either effect leads to a lower effective slip length than that predicted by assuming an ideal flat and no-shear interface. Cheng *et al.*[8] found from their numerical simulations that for a gas/liquid viscosity ratio not larger than $O(0.01)$, the result is not appreciably different from that based on a shear-free interface.

Despite these studies, the liquid-gas shear effect on the slip length is yet to be fully understood. This has motivated the present study. Like many previous studies,[6,9–11] the present problem is to consider flow through a channel bounded by two plane walls, each of which is micropatterned with a periodic array of ribs and grooves aligned either parallel or normal to the principal flow direction. Our objectives here are to develop analytical models that can simulate finite shear on the liquid-gas interface and to examine how the gas viscosity may affect the slip lengths as a function of various parameters in the problem.

Davies *et al.*[10] and Maynes *et al.*[11] performed similar studies on the comparison between predictions by a zero-interfacial-shear model and a liquid-gas coupled model. With an intention to achieve a wider scope, our study is different from theirs in the following aspects. First, in their simulations, they considered only a single value of the gas viscosity (equal to that of air at standard conditions) and hence did not examine the results as a function of the gas/liquid viscosity ratio. We shall show that the prediction under some conditions can be very sensitive to the viscosity ratio. Second,

a)Author to whom correspondence should be addressed. Electronic mail: cong@hku.hk.

intrinsic slippage was ignored in their study, but is considered as one of the controlling parameters in the present study. We shall show that even a small amount of intrinsic slippage can have a nontrivial influence by amplifying the effect of gas viscosity on the slip length. Third, they normalized the length quantities with respect to the hydraulic diameter, while we choose to normalize the length quantities by half the pattern period. Results in terms of different normalized parameters can reveal a relationship from a different perspective. Our results can directly reflect the individual dependence of the slip lengths on the channel height and the groove depth. Finally, the liquid-gas coupled model of Maynes *et al.*[11] is analytical (by series expansions) only in the gas domain, but numerical (by finite elements) in the liquid domain. Davies *et al.*[10] solved the problem numerically using a commercial computational fluid dynamics (CFD) code. According to their own description, their solution procedure required several hundred thousand iterations (apparently because of the weak coupling due to small shear on the interface), which took them five to ten days to accomplish one simulation for longitudinal flow,[11] and 10 to 15 days to accomplish one simulation for transverse flow.[10] In sharp contrast, our model is analytical in both liquid and gas domains. Following Wang[12] and Ng and Wang,[13] we express the velocity components by eigenfunction expansions, where the unknown coefficients are determined by the matching of velocities and shear stresses on the interface. Our model, which generates results very quickly on a personal computer (PC), is much more efficient than the models by Davies *et al.*[10] and Maynes *et al.*[11] They deduced the slip length by taking section-average of the numerically obtained velocity. In our model, the slip length is obtained directly as part of the solution.

II. COUPLED MODELS AND SOLUTIONS

We consider pressure-driven viscous flow of a liquid through a plane channel bounded by two parallel superhydrophobic surfaces that are fabricated with a periodic pattern of ribs and grooves, running either along or normal to the axis of the channel (Fig. 1). In this study, it is assumed that the liquid does not penetrate the grooves, which are completely filled with a gas. The liquid-gas interface is idealized to be a flat surface lying on the top of the ribs and, therefore, aligns with the liquid-solid interface. The meniscus curvature effect is not considered in this study. As remarked by Maynes *et al.*,[11] a flat interface is an idealization representing only one of many possible curvatures. The actual interface curvature depends on the local pressure differential between the liquid and the gas phases, which is assumed to be small here in order to justify the assumption of a flat interface. Near the entrance of the channel, the pressure can be so high that the liquid impregnates the grooves, for which the present models are not valid.

We further assume that, by virtue of the small length scales of the problem, the Reynolds number, Re, is very small and the flow is governed by the noninertial Stokes equation. As shown by Cheng *et al.*,[8] the slip lengths will not be materially affected by the Reynolds number as long as it is not greater than $O(100)$. Here, we assume that $\mathrm{Re} \ll 1$.

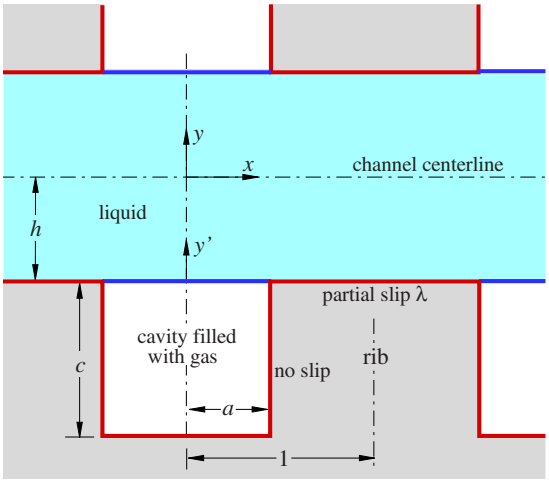

FIG. 1. (Color online) Flow through a plane channel with grooved walls; longitudinal flow is normal to the $x-y$ plane, while transverse flow is along the x-axis. The coordinates and length dimensions are normalized with respect to half the period of the wall pattern. The liquid-gas interface is a flat surface in alignment with the top of the ribs.

The problems presented below are formulated in terms of nondimensional quantities; the lengths are normalized by L, while the velocities are normalized by KL^2/μ_l, where L is half the pattern periodicity (or pitch), K is the axial pressure gradient applied to the liquid, and μ_l is the liquid viscosity. The ratio of gas viscosity to liquid viscosity is denoted by $\mu \equiv \mu_g/\mu_l$, where μ_g is the gas viscosity. Unless stated otherwise, we shall from here on use only nondimensional quantities.

Shown in Fig. 1 is one unit of the periodic structure of the channel cross section, which is characterized by the following lengths (which are normalized by half the pitch of the wall pattern): h=half the channel height, a=half the groove width, and c=depth of the gas cavity. Only in-phase arrangement of the pattern on the two walls is considered in this work. The flow is, therefore, symmetrical about the centerline of the channel. Note that a also represents the area fraction of the wall where the liquid is cushioned by the gas. Owing to the lubrication resulting from a small ratio of gas viscosity to liquid viscosity, $\mu \ll 1$, the liquid flow experiences wall slip, thereby a reduction in flow resistance. It is also possible that the solid phase is chemically treated to exhibit intrinsic slippage. We here allow a finite intrinsic slip length $\lambda \geq 0$ along the liquid-solid interface, while the gas-solid interface is always nonslip. It is the combined effect due to the gas cushioning over the grooves and the intrinsic slippage over the ribs that will determine the overall effective slip of the liquid over the composite wall.

A. Longitudinal flow

Let us first consider a pressure gradient $K=-dp_l/dz$ (dimensional) that is normal to the $x-y$ plane shown in Fig. 1 and the flow is hence in a direction parallel to the grooves and ribs. For convenience, we develop solutions for the liq-

uid and the gas flows in terms of the wall-normal coordinates y and y', respectively, which are defined in Fig. 1.

The liquid flow is governed by

$$\frac{\partial^2 w_l}{\partial x^2} + \frac{\partial^2 w_l}{\partial y^2} = -1, \tag{1}$$

where $w_l(x,y)$ is the liquid velocity. The solution is composed of the basic Poiseuille flow, a slip flow, and a periodic flow that is even in both x and y,

$$w_l(x,y) = \frac{h^2}{2}\left(1 - \frac{y^2}{h^2}\right) + h\delta_{\|} + h\sum_{n=1}^{\infty} C_n \cos(\gamma_n x)\frac{\cosh(\gamma_n y)}{\cosh(\gamma_n h)}, \tag{2}$$

where $\delta_{\|}$ is the longitudinal macroscopic slip length, C_n are unknown coefficients, and $\gamma_n = n\pi$.

Following Maynes *et al.*,[11] we suppose that the gas cavity is closed at the two axial ends of the channel, and the net cross-sectional flux of the gas phase is zero. A positive pressure gradient $dp_g/dz = \mu GK$ (dimensional) is induced in the gas to produce backward flow balancing the forward flow caused by the interfacial stress. As a result, a recirculation convection cell develops along the entire length of the cavity. For sufficiently far from the end walls, the gas flow is governed by

$$\frac{\partial^2 w_g}{\partial x^2} + \frac{\partial^2 w_g}{\partial y'^2} = G, \tag{3}$$

where $w_g(x,y')$ is the gas velocity. The solution, which is even in x and satisfies no-slip at the cavity bottom $w_g(x,-c)=0$, can be written as follows:

$$w_g(x,y') = \frac{Gc^2}{2}\left(\frac{y'^2}{c^2} + \frac{y'}{c}\right) + h\sum_{n=1}^{\infty} A_n \cos(\alpha_n x)[e^{\alpha_n y'} - e^{-\alpha_n(y'+2c)}] + h\sum_{n=1}^{\infty} B_n \sin(\beta_n y')\frac{\cosh(\beta_n x)}{\cosh(\beta_n a)}, \tag{4}$$

where A_n and B_n are unknown coefficients, $\alpha_n = (n-1/2)\pi/a$, and $\beta_n = n\pi/c$.

Using the zero-flux condition, $\int_{-c}^{0}\int_{0}^{a} w_g dx dy' = 0$, the induced pressure gradient G can be related to A_n and B_n as below

$$\frac{ac}{12h}G = \sum_{n=1}^{N}\frac{A_n}{(\alpha_n c)^2}\sin(\alpha_n a)(1 - e^{-\alpha_n c})^2 - \sum_{n=1}^{P}\frac{B_n}{(\beta_n c)^2}\tanh(\beta_n a)[1 - \cos(\beta_n c)], \tag{5}$$

where the coefficients A_n and B_n are truncated to N and P terms, respectively.

By the no-slip condition on the lateral wall of the cavity, and using orthogonality of the eigenfunctions, we obtain from $\int_{-c}^{0} w_g(a,y')\sin(\beta_m y')dy' = 0$,

$$B_m = -\frac{2G}{ch\beta_m^3}[1 - \cos(\beta_m c)] \quad (m = 1, \ldots, P). \tag{6}$$

On substituting this into Eq. (5), we get

$$G = \frac{12h}{ac\zeta}\sum_{n=1}^{N}\frac{\sin(\alpha_n a)}{(\alpha_n c)^2}(1 - e^{-\alpha_n c})^2 A_n, \tag{7}$$

where

$$\zeta = 1 - 24\sum_{n=1}^{P}\frac{\tanh(\beta_n a)[1 - \cos(\beta_n c)]^2}{(\beta_n a)(\beta_n c)^4}. \tag{8}$$

The matching conditions on the liquid-gas and liquid-solid interfaces are

$$w_l|_{y=-h} = \begin{cases} w_g|_{y'=0} & (0 \le x < a) \\ \lambda\, \partial w_l/\partial y|_{y=-h} & (a < x \le 1), \end{cases} \tag{9}$$

$$\left.\frac{\partial w_l}{\partial y}\right|_{y=-h} = \mu \left.\frac{\partial w_g}{\partial y'}\right|_{y'=0} \quad (0 \le x < a), \tag{10}$$

where $\mu = \mu_g/\mu_l$ is the viscosity ratio, and λ is the intrinsic slip length on the liquid-solid surface. Integrating Eq. (9) with respect to x from 0 to 1 gives

$$\delta_{\|} = \sum_{n=1}^{N}\frac{\sin(\alpha_n a)}{\alpha_n}(1 - e^{-2\alpha_n c})A_n + \lambda \times\left[1 - a + \sum_{n=1}^{M}\tanh(\gamma_n h)\sin(\gamma_n a)C_n\right], \tag{11}$$

where C_n are truncated to M terms. Multiplying Eq. (9) by $\cos(\gamma_m x)$ and integrating with respect to x from 0 to 1 gives

$$\sum_{n=1}^{N} I_{mn}(1 - e^{-2\alpha_n c})A_n - \lambda\sum_{n=1}^{M}\gamma_n J_{mn}\tanh(\gamma_n h)C_n - \frac{1}{2}C_m = \lambda\frac{\sin(\gamma_m a)}{\gamma_m} \quad (m = 1, \ldots, M), \tag{12}$$

where

$$I_{mn} = \begin{cases} \dfrac{\alpha_n}{\alpha_n^2 - \gamma_m^2}\sin(\alpha_n a)\cos(\gamma_m a) & \text{if } \gamma_m \ne \alpha_n \\ \dfrac{a}{2} & \text{if } \gamma_m = \alpha_n, \end{cases} \tag{13}$$

$$J_{mn} = \begin{cases} -\dfrac{\sin[(\gamma_m - \gamma_n)a]}{2(\gamma_m - \gamma_n)} - \dfrac{\sin[(\gamma_m + \gamma_n)a]}{2(\gamma_m + \gamma_n)} & \text{if } m \ne n \\ \dfrac{1-a}{2} - \dfrac{\sin(2\gamma_m a)}{4\gamma_m} & \text{if } m = n. \end{cases} \tag{14}$$

We next multiply Eq. (10) by $\cos(\alpha_m x)$ and integrate it with respect to x from 0 to a to get

$$\mu\frac{c}{2h}\frac{\sin(\alpha_m a)}{\alpha_m}G+\mu\frac{\alpha_m a}{2}(1+e^{-2\alpha_m c})A_m + \mu\sum_{n=1}^{P}\left(\frac{\alpha_m\beta_n}{\alpha_m^2+\beta_n^2}\right)\sin(\alpha_m a)B_n + \sum_{n=1}^{M}\gamma_n I_{nm}\tanh(\gamma_n h)C_n = \frac{\sin(\alpha_m a)}{\alpha_m} \quad (m=1,\ldots,N). \tag{15}$$

Equations (6), (7), (12), and (15) form a system of $N+P+M+1$ linear equations that can be solved for the same number of unknowns: $A_{1,\ldots,N}$, $B_{1,\ldots,P}$, $C_{1,\ldots,M}$, and G. The longitudinal slip length $\delta_\parallel$ is then available from Eq. (11). In this work, we used the IMSL-DLSARG FORTRAN high-precision solver to solve the system of equations. The numbers of terms required to achieve good accuracy depend on the viscosity ratio μ; the smaller the μ, the greater the numbers of terms required. We have found that for $\mu=O(0.01)$, we need $N=O(400)$, $P=O(200)$, and $M=O(200)$ to achieve an accuracy of 0.1%. It typically took a few seconds to get a solution on a PC.

The limiting case of zero-shear on the liquid-gas interface, $\mu=0$, is of interest to us. The system of equations deduced above will, however, converge slowly as $\mu\to 0$ when the coupling between liquid and gas diminishes. To solve for this limit in a more direct and simpler manner, the liquid flow is found by the method of collocation instead. The coefficients $C_{1,\cdots,M}$ and $\delta_\parallel$ are to be determined by having the composite boundary condition

$$\left.\begin{array}{ll}\partial w_l/\partial y=0, & 0\le x<a\\ w_l-\lambda\,\partial w_l/\partial y=0, & a<x\le 1\end{array}\right\} y=-h, \tag{16}$$

to be satisfied at equidistant $M+1$ discrete points on the line $0\le x\le 1$, $y=-h$.

For the ideal case of zero-gas viscosity and a thick channel ($\mu=0$, $\lambda=0$, and $h\gg 1$), the flow amounts to shear flow over a flat plate with a periodic array of no-shear alternating with no-slip slots. The macroscopic slip length has been analytically deduced by Philip[14]

$$\delta_{\parallel ZS}^{\text{plate}}=\frac{2}{\pi}\ln\left[\sec\left(\frac{\pi a}{2}\right)\right] \quad (\mu=0,\quad \lambda=0,\quad h\gg 1). \tag{17}$$

B. Transverse flow

We next consider liquid flow that is driven by $K=-dp_l/dx$ (dimensional) and is in a direction normal to the grooves and ribs. The governing equations of motion are the continuity equation $\partial u/\partial x+\partial v/\partial y=0$ and the Stokes equation $\nabla^2(u,v)=\nabla p$, where u and v are the x- and y-components of velocity.

In the liquid domain, the pressure gradient is $\nabla p=(-1+\partial p_l/\partial x,\partial p_l/\partial y)$, where p_l is a periodic odd function of x. The x-velocity is even in both x and y, while the y-velocity is odd in both x and y. The basic expressions satisfying zero normal velocity at the walls ($v_l=0$ at $y=\pm h$) are

$$u_l(x,y)=\frac{h^2}{2}\left(1-\frac{y^2}{h^2}\right)+h\delta_\perp+h\sum_{n=1}^{\infty}\frac{\cos(\gamma_n x)}{\cosh(\gamma_n h)}E_n \times\{\gamma_n h\cosh(\gamma_n y)-\tanh(\gamma_n h)[\cosh(\gamma_n y)+\gamma_n y\sinh(\gamma_n y)]\}, \tag{18}$$

$$v_l(x,y)=h\sum_{n=1}^{\infty}\frac{\sin(\gamma_n x)}{\cosh(\gamma_n h)}E_n[\gamma_n h\sinh(\gamma_n y)-\gamma_n y\tanh(\gamma_n h)\cosh(\gamma_n y)], \tag{19}$$

where $\delta_\perp$ is the transverse macroscopic slip length, E_n are unknown coefficients, and $\gamma_n=n\pi$.

Gas flow in the cavity is recirculatory in the $x-y$ plane. The x-velocity is even in x, while the y-velocity is odd in x. The velocity components that satisfy zero normal velocity at the boundaries ($u_g=0$ at $x=\pm a$, and $v_g=0$ at $y'=0,-c$) are

$$u_g(x,y')=h\sum_{n=1}^{\infty}\frac{\cos(\alpha_n x)}{\alpha_n\cosh(\alpha_n c)}[A_n F_n'(y')+B_n G_n'(y')]+h\sum_{n=1}^{\infty}\cos(\beta_n y')D_n H_n(x), \tag{20}$$

$$v_g(x,y')=h\sum_{n=1}^{\infty}\frac{\sin(\alpha_n x)}{\cosh(\alpha_n c)}[A_n F_n(y')+B_n G_n(y')]-h\sum_{n=1}^{\infty}\sin(\beta_n y')\frac{D_n}{\beta_n}H_n'(x), \tag{21}$$

where A_n, B_n, and D_n are unknown coefficients, $\alpha_n=(n-1/2)\pi/a$, and $\beta_n=n\pi/c$. The three functions in these expressions are

$$F_n(y')=\sinh(\alpha_n y')-\sinh(\alpha_n c)(y'/c)e^{-\alpha_n(y'+c)}, \tag{22}$$

$$G_n(y')=\alpha_n y'\sinh[\alpha_n(y'+c)], \tag{23}$$

$$H_n(x)=e^{\beta_n(x-a)}+e^{-\beta_n(x+a)}-\frac{(1+e^{-2\beta_n a})x}{a(1-e^{-2\beta_n a})}\times[e^{\beta_n(x-a)}-e^{-\beta_n(x+a)}]. \tag{24}$$

The following boundary or matching conditions are yet to be satisfied:

$$u_g=0 \quad (y'=-c), \tag{25}$$

$$v_g=0 \quad (x=a), \tag{26}$$

$$u_l|_{y=-h}=\begin{cases}u_g|_{y'=0} & (0\le x<a)\\ \lambda\,\partial u_l/\partial y|_{y=-h} & (a<x\le 1),\end{cases} \tag{27}$$

$$\left.\frac{\partial u_l}{\partial y}\right|_{y=-h} = \mu \left.\frac{\partial u_g}{\partial y'}\right|_{y'=0} \quad (0 \le x < a). \tag{28}$$

Let us truncate A_n and B_n each to N terms, D_n to P terms, and E_n to M terms.

Multiplying Eq. (25) by $\cos(\alpha_m x)$ and integrating with respect to x from 0 to a gives

$$a[1-(1+(\alpha_m c)^{-1})\tanh(\alpha_m c)]A_m - a\alpha_m c\ \mathrm{sech}(\alpha_m c)B_m + 2\sum_{n=1}^{P} \frac{2\alpha_m\beta_n(1+e^{-2\beta_n a})^2\sin(\alpha_m a)\cos(\beta_n c)}{a(1-e^{-2\beta_n a})(\alpha_m^2+\beta_n^2)^2} \times D_n = 0 \quad (m=1,\ldots,N). \tag{29}$$

Multiplying Eq. (26) by $\sin(\beta_m y')$ and integrating with respect to y' from $-c$ to 0 gives

$$\sum_{n=1}^{N} \frac{2\alpha_n\beta_m\sin(\alpha_n a)}{c(\alpha_n^2+\beta_m^2)^2}\{\tanh(\alpha_n c)[e^{-\alpha_n c}-\cos(\beta_m c)]A_n + \alpha_n c \times[1-\mathrm{sech}(\alpha_n c)\cos(\beta_m c)]B_n\} + \frac{c}{2}\left[\frac{4\beta_m a e^{-2\beta_m a}-e^{-4\beta_m a}+1}{\beta_m a(1-e^{-2\beta_m a})}\right]D_m = 0 \quad (m=1,\ldots,P). \tag{30}$$

Integrating Eq. (27) with respect to x from 0 to 1 gives

$$\delta_\perp = \sum_{n=1}^{N}\frac{\sin(\alpha_n a)}{\alpha_n}\left[\left(\mathrm{sech}(\alpha_n c)-\frac{\tanh(\alpha_n c)}{\alpha_n c}e^{-\alpha_n c}\right)A_n + \tanh(\alpha_n c)B_n\right] + \sum_{n=1}^{P}\left[\frac{1-e^{-4\beta_n a}-4\beta_n a e^{-2\beta_n a}}{\beta_n^2 a(1-e^{-2\beta_n a})}\right]D_n + \lambda\left[1-a-2\sum_{n=1}^{M}\tanh^2(\gamma_n h)\sin(\gamma_n a)E_n\right]. \tag{31}$$

Multiplying Eq. (27) by $\cos(\gamma_m x)$, followed by integration with respect to x from 0 to 1, we obtain

$$\sum_{n=1}^{N} I_{mn}\left[\left(\mathrm{sech}(\alpha_n c)-\frac{\tanh(\alpha_n c)}{\alpha_n c}e^{-\alpha_n c}\right)A_n + \tanh(\alpha_n c)B_n\right] + \sum_{n=1}^{P}\hat{H}_{mn}D_n + 2\lambda\sum_{n=1}^{M}\gamma_n J_{mn}\tanh^2(\gamma_n h)E_n - \frac{1}{2}[\gamma_m h\ \mathrm{sech}^2(\gamma_m h)-\tanh(\gamma_m h)]E_m = \lambda\frac{\sin(\gamma_m a)}{\gamma_m} \quad (m=1,\ldots,M), \tag{32}$$

where I_{mn} and J_{mn} are, respectively, given in Eqs. (13) and (14), and

$$\hat{H}_{mn} = \frac{1}{a(1-e^{-2\beta_n a})(\beta_n^2+\gamma_m^2)^2} \times\{2\gamma_m\beta_n(1+e^{-2\beta_n a})^2\sin(\gamma_m a) + [(\beta_n^2-\gamma_m^2)(1-e^{-4\beta_n a}) - 4\beta_n a(\beta_n^2+\gamma_m^2)e^{-2\beta_n a}]\cos(\gamma_m a)\}. \tag{33}$$

Finally, multiplying Eq. (28) by $\cos(\alpha_m x)$, followed by integration with respect to x from 0 to a, we get

$$\mu a\alpha_m\left[\frac{\tanh(\alpha_m c)}{\alpha_m c}e^{-\alpha_m c}A_m + B_m\right] - 2\sum_{n=1}^{M}\gamma_n I_{nm}\tanh^2(\gamma_n h)E_n = \frac{\sin(\alpha_m a)}{\alpha_m} \quad (m=1,\ldots,N). \tag{34}$$

Equations (29), (30), (32), and (34) are a system of $2N+P+M$ linear equations for the unknowns: $A_{1,\ldots,N}$, $B_{1,\ldots,N}$, $D_{1,\ldots,P}$, and $E_{1,\ldots,M}$. The transverse slip length $\delta_\perp$ is calculated by Eq. (31). Again, the IMSL-DLSARG high-precision solver was employed to solve the system of equations. The numbers of terms required to achieve good accuracy are comparable to those in the longitudinal case. The limiting case of $\mu=0$ is again solved in a simpler manner using the method of collocation. The coefficients $E_{1,\ldots,M}$ and $\delta_\perp$ are determined by forcing the composite boundary condition to be satisfied at $M+1$ discrete points on the wall. For the ideal case of zero-gas viscosity and a thick channel ($\mu=0$, $\lambda=0$, and $h \gg 1$), the macroscopic slip length has also been analytically deduced by Philip,[14]

$$\delta_{\perp ZS}^{\mathrm{plate}} = \frac{1}{\pi}\ln\left[\sec\left(\frac{\pi a}{2}\right)\right] \quad (\mu=0, \quad \lambda=0, \quad h \gg 1), \tag{35}$$

which is exactly equal to half $\delta_{\parallel ZS}^{\mathrm{plate}}$ given in Eq. (17).

III. RESULTS

The problems are solved with the following inputs: channel height (h), the gas area fraction of the wall (a), the depth of gas cavity (c), the viscosity ratio (μ), and the intrinsic slip length (λ). Typical values of viscosity are $O(10^{-3})$ and $O(10^{-5})$ Pa s for liquids and gases, respectively. Therefore, it is reasonable to assume that $\mu=O(10^{-2})$. We ask the question: under what conditions will such a small viscosity ratio lead to nonsmall effects on the slip lengths? We have checked that our analytical models are capable of producing results that agree favorably with those known or published in the literature. Our results are in excellent agreement in the zero-gas-viscosity limit when compared with the two analytical expressions given in Eqs. (17) and (35) for flow over a plate, and with the results by the analytical model of Teo and Khoo[6] for flow through a channel. Our results also agree reasonably well with those computed numerically by Davies *et al.*[10] and Maynes *et al.*[11]

We show in Fig. 2, for both longitudinal and transverse flows, the liquid phase velocity profiles on the liquid-gas interface at $y=-h$, where $a=0.875, 0.75, 0.5$, $c=0.8$, $\lambda=0$, and $\mu=0$ (solid), 0.01 (dashed), 0.02 (dashed-dotted). The channel height is $h=2$, except in one case, $h=10$, as specified in Fig. 2(b). The symbols are the results adopted from previous studies: crosses denote the zero-shear model by Teo and Khoo,[6] squares and circles denote, respectively, the zero-shear model and the liquid-gas coupled model by Maynes

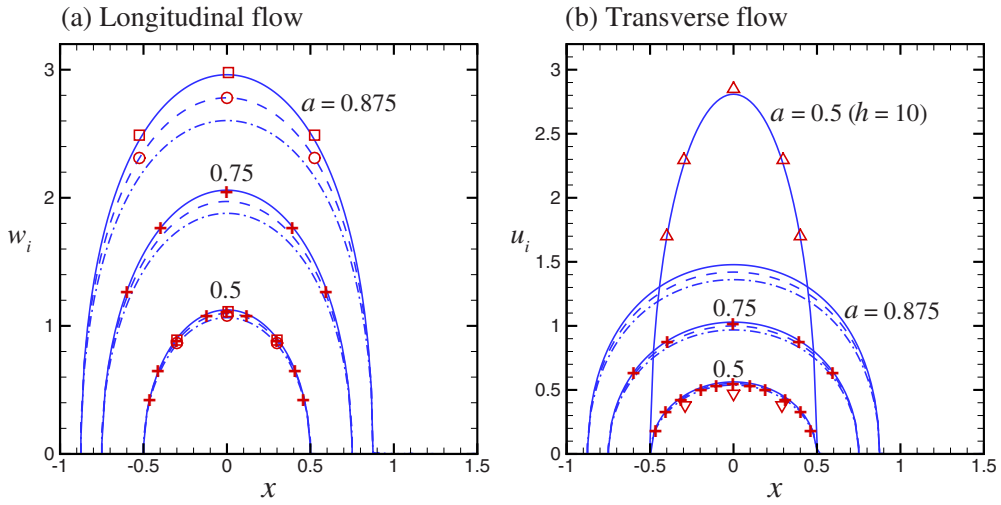

FIG. 2. (Color online) Streamwise velocity profiles of the liquid phase on the liquid-gas interface for (a) longitudinal flow, (b) transverse flow, where $a=0.875, 0.75, 0.5$, $c=0.8$, $\lambda=0$, and $\mu=0$ (solid), 0.01 (dashed), 0.02 (dashed-dotted). The channel height is $h=2$, except in one case, $h=10$, as specified in (b). The symbols are the results adopted from previous studies: Teo and Khoo (Ref. 6) (crosses), Maynes *et al.* (Ref. 11) (squares and circles), and Davies *et al.* (Ref. 10) (triangles and inverted triangles).

et al.,[11] triangles and inverted triangles denote, respectively, the zero-shear model and the liquid-gas coupled model (only the low-Reynolds-number cases are selected here) by Davies *et al.*[10] The close agreement between our model and that of Teo and Khoo[6] is clearly demonstrated. Both models solve Stokes flow analytically using Fourier series expansions, and hence agreement in results is somewhat expected. Our results also largely accord with the results obtained by Davies *et al.*[10] and Maynes *et al.*,[11] who solved the Navier–Stokes equations with CFD codes. The agreement with these CFD results is mostly within 3%, although in the case $a=0.5$ of transverse flow, the peak interfacial velocity obtained by Davies *et al.*[10] is some 13% lower than that calculated by both the present model and the model of Teo and Khoo.[6]

We also note that, as already pointed out by Teo and Khoo,[6] the interfacial velocity of longitudinal flow is nearly twice in magnitude that of the corresponding transverse flow. We further note that the interfacial velocity can be materially decreased by a viscosity ratio as small as 0.01–0.02 when a is sufficiently large, say $a>0.5$. Here, the longitudinal flow is subject to a greater decreasing effect due to gas viscosity than the transverse flow. Such dependence of the flow on the viscosity ratio will be further examined when the effective slip lengths are discussed below.

A. Longitudinal slip length

Figure 3 shows the longitudinal effective slip length $\delta_\parallel$ as a function of h and a, where $\mu=0.01$ and $\lambda=0$. Part (a) of the figure is for a deep gas cavity $c=2$ and part (b) is for a shallower gas cavity $c=0.2$. One can infer from previous results by Wang[12] that a groove can be considered to be deep (i.e., its bottom is not felt by the flow outside the groove) when its depth is equal to or greater than its width. For comparison, the corresponding results for ideal zero-gas viscosity, $\mu=0$, are shown by the dashes in the figure. These dashes approach on their right ends the analytical limits given by Eq. (17). One can clearly see that the slip length $\delta_\parallel$ is virtually not affected by the channel height as long as the height $h>0.5$. In fact, the use of a very thin channel (say $h<0.5$) may not be practically desirable as the pressure required to drive the flow can be so large that the capillary

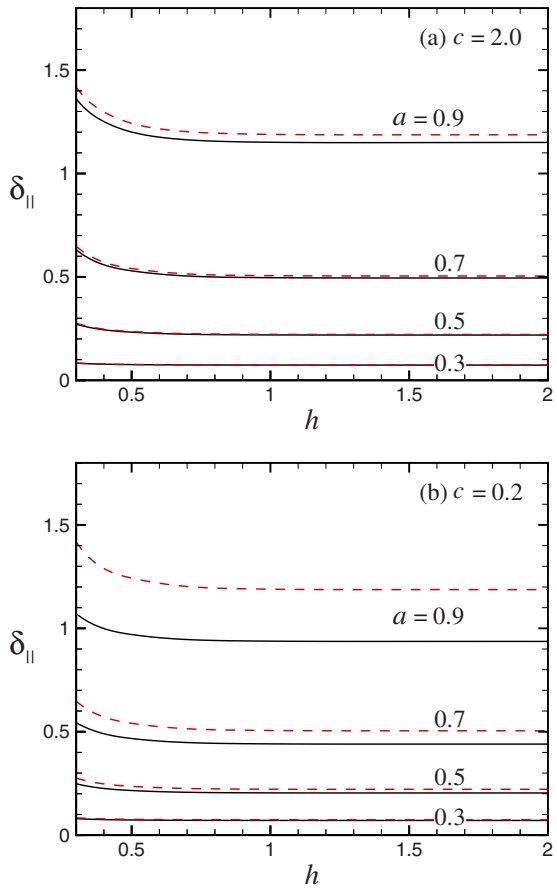

FIG. 3. (Color online) Longitudinal slip length $\delta_\parallel$ as a function of the channel height h and gas area fraction of the wall a, where $\lambda=0$, $\mu=0.01$, and (a) $c=2$, (b) $c=0.2$. The dashes are for ideal gas $\mu=0$.

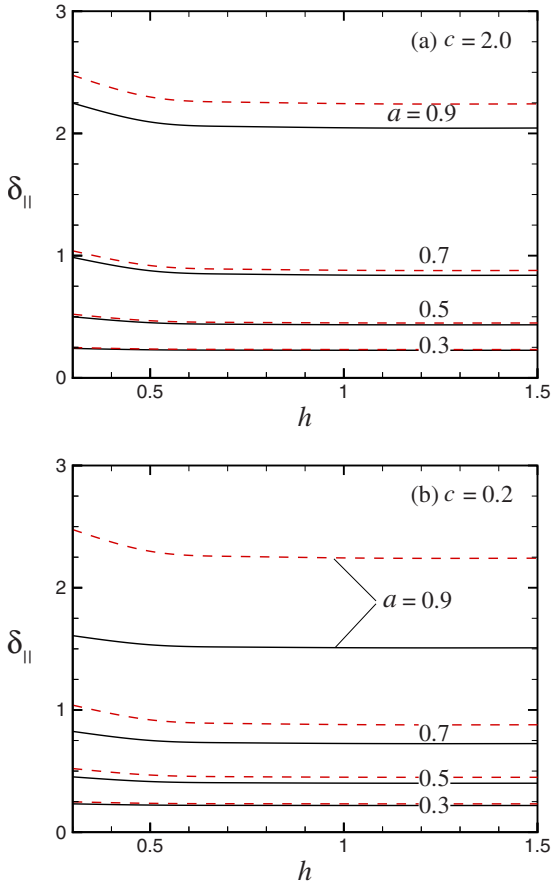

FIG. 4. (Color online) Longitudinal slip length $\delta_\parallel$ as a function of the channel height h and gas area fraction of the wall a, where $\lambda=0.1$, $\mu=0.01$, and (a) $c=2$, (b) $c=0.2$. The dashes are for ideal gas $\mu=0$.

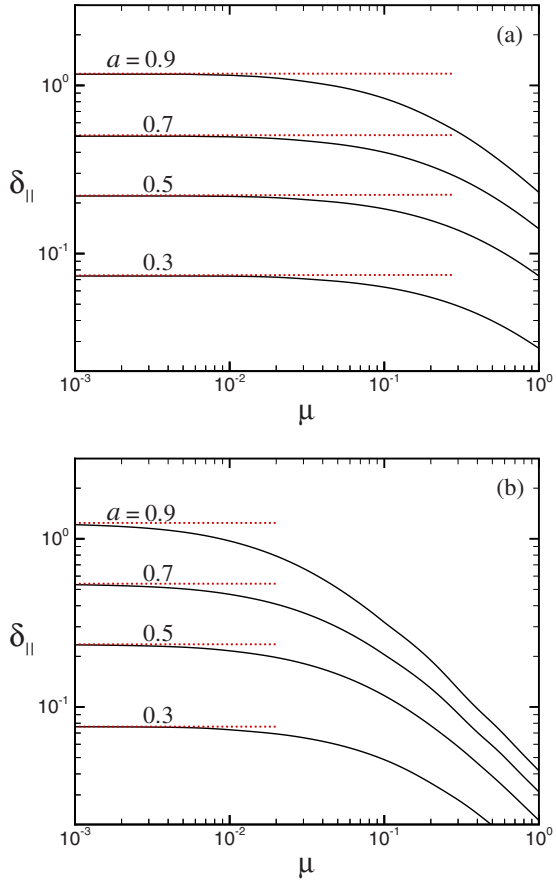

FIG. 5. (Color online) Longitudinal slip length $\delta_\parallel$ as a function of the viscosity ratio μ and gas area fraction of the wall a, where $\lambda=0$, and (a) $h=5$, $c=2$, (b) $h=0.5$, $c=0.2$. The dotted lines are the limits for ideal gas $\mu=0$.

pressure will be exceeded and thereby the superhydrophobic state will be lost. We shall focus on $h \geq 0.5$ in this study.

The gas shear effect on the slip length is indeed very small for sufficiently large h and c, even when a is close to unity; see Fig. 3(a). However, the gas viscous effect becomes non-negligible when the grooves are shallow. Figure 3(b) shows that a small but finite value of $\mu=0.01$ may predict a slip length some 20% lower than that by the idealized zero-shear model when $a=0.9$ and $h \geq 0.5$. The percentage difference increases as h decreases, but decreases as a decreases. For a small gas area fraction $a<0.5$, the gas shear will have practically negligible effect unless $c \ll 1$. These observations are basically consistent with those reported by Davies *et al.*[10] and Maynes *et al.*,[11] although their results were presented in terms of different normalized quantities.

Figure 4 shows similar plots, but for $\lambda=0.1$. Remarkably, even such a small value of intrinsic slippage will greatly magnify the gas viscous effect on the slip length, especially for $a>0.5$. Even for a deep groove, the idealized no-shear model will significantly overpredict the slip length (by 10% for $a=0.9$) under the influence of the intrinsic slippage. The difference is much larger (by 50% for $a=0.9$) for a shallow groove of $c=0.2$.

The dependence of the slip length on the viscosity ratio is shown in Fig. 5. Part (a) of the figure is for a deep groove and a thick channel ($c=2$, $h=5$), while part (b) is for a shallow groove and a thinner channel ($c=0.2$, $h=0.5$). In the case of a deep groove, the zero-shear model is a very good approximation as long as $\mu \leq O(10^{-2})$, for which the gas shear is too small to have appreciable effect on the slip length for any $a<1$. In the case of a shallow groove, the zero-gas-shear model is a good approximation only for much smaller μ, especially for large a. For $a=0.9$, there is already a 20% overprediction by the idealized zero-shear model when μ is only as small as 0.01.

The point that the slip length is sensitive to the viscosity ratio when the grooves are shallow is further illustrated in Fig. 6, where $a=0.9$, $h=0.5$, and $\lambda=0$. For $c=0.2$, the slip length is some 20%–36% lower than the idealized value when the viscosity ratio μ varies mildly from 0.01 to 0.02.

B. Transverse slip length

Plots like Figs. 3–5, but for the transverse effective slip length $\delta_\perp$, are shown in Figs. 7–9. On comparing Figs. 3 and 7, one finds that, unlike $\delta_\parallel$, $\delta_\perp$ decreases with decreasing h. Also, the overprediction by the no-shear model diminishes as h decreases. Except for these behaviors with small h, the observations made above regarding the longitudinal slip length apply also to the transverse slip length. A viscosity ratio, as small as $\mu=0.01$, will have non-negligible effect when the grooves are shallow ($c<0.5$) and the gas area frac-

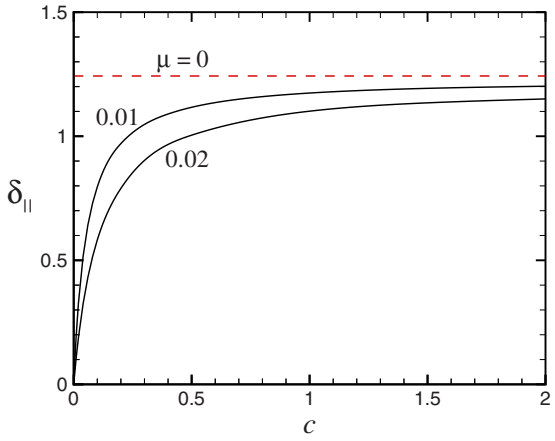

FIG. 6. (Color online) Longitudinal slip length $\delta_{\|}$ as a function of the groove depth c, for $\mu=0,0.01,0.02$, where $\lambda=0$, $a=0.9$, and $h=0.5$.

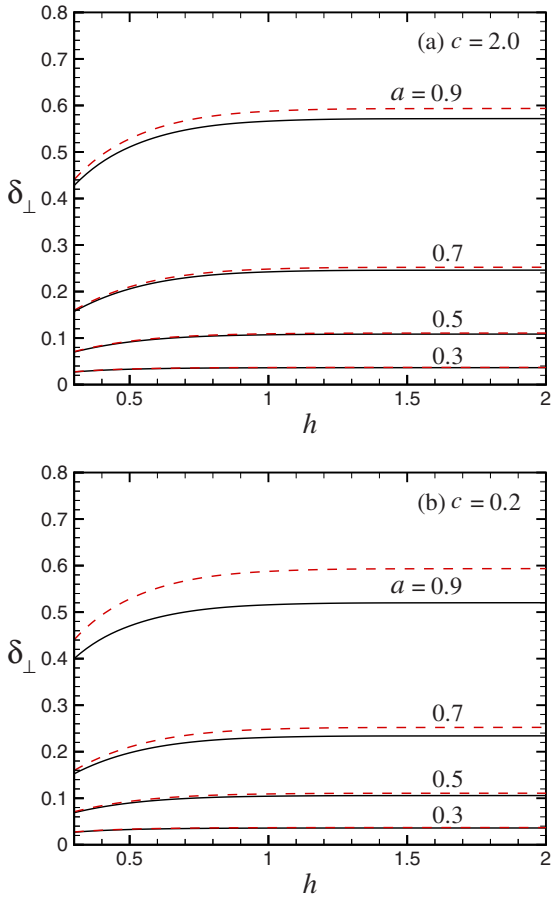

FIG. 7. (Color online) Transverse slip length $\delta_{\perp}$ as a function of the channel height h and gas area fraction of the wall a, where $\lambda=0$, $\mu=0.01$, and (a) $c=2$, (b) $c=0.2$. The dashes are for ideal gas $\mu=0$.

tion of the wall is large ($a>0.5$). The decreasing effect of nonzero-gas shear on the effective slip length can be dramatically magnified by the intrinsic liquid slippage on the ribs. Figure 9(b) shows that, in the presence of intrinsic slippage, the macroscopic slip length is very sensitively affected by even a small value of gas viscosity. Under these conditions, the no-shear model will fall short in accurately predicting the slip length. The liquid-gas coupling needs to be taken into account in the modeling.

We further illustrate how the intrinsic slip length may affect the effective slip length in Fig. 10, where $a=0.9$, $c=2$, and $h=5$. It is clearly seen that, with even a modest amount of intrinsic slippage, the slip length is sensitively decreased by the gas viscosity. For example, for $\lambda=0.1$, a viscosity ratio as small as 0.005–0.02 will lower the slip length by some 9%–26% compared with that by the idealized model. Let us explain this in terms of the so-called local slip length over the gas phase λ_g. Such a local slip length can be defined as the ratio of the averaged slip velocity to the averaged velocity gradient over the liquid-gas interface,

$$\lambda_g = \frac{\int_0^a u_l|_{y=-h}dx}{\int_0^a \partial u_l/\partial y|_{y=-h}dx} = \frac{\delta_\perp + \Sigma_{n=1}^M \sin(\gamma_n a)[\gamma_n h\ \mathrm{sech}^2(\gamma_n h) - \tanh(\gamma_n h)]E_n/(\gamma_n a)}{1 + 2\Sigma_{n=1}^M \tanh^2(\gamma_n h)\sin(\gamma_n a)E_n/a}. \tag{36}$$

Following previous researchers,[15,16] we may write, as a first approximation,

$$\frac{1}{\delta_{\mathrm{eff}}} \approx \frac{1-a}{\lambda} + \frac{a}{\lambda_g} \quad \text{for} \quad \lambda > 0. \tag{37}$$

For ideal gas $\mu=0$, λ_g is infinite, so the second term above vanishes. Even for real gas with sufficiently small viscosity $\mu\sim 0$, λ_g is finite but can be so large that the second term above is still subdominant. Under these conditions, the effective slip length remains largely unaffected by the gas viscosity. One has, however, yet to determine the rate by which the gas slip length λ_g is affected by the viscosity ratio μ under the influence of intrinsic slippage.

One may regard the reciprocal of the gas slip length λ_g^{-1} as the surface friction over the liquid-gas interface.[7,15] Figure 10(b) shows how λ_g^{-1} varies with λ for several small values of μ. Indeed, the gas friction coefficient increases at a sharp rate with the viscosity ratio. Even for a viscosity ratio as small as 0.01, it is very easy for the two terms in Eq. (37) to be comparable with each other. The intrinsic slip is to reduce the friction over the solid phase, but is to increase the friction over the gas phase. In other words, for a sufficiently large gas area fraction of the wall, it is probable that the flow

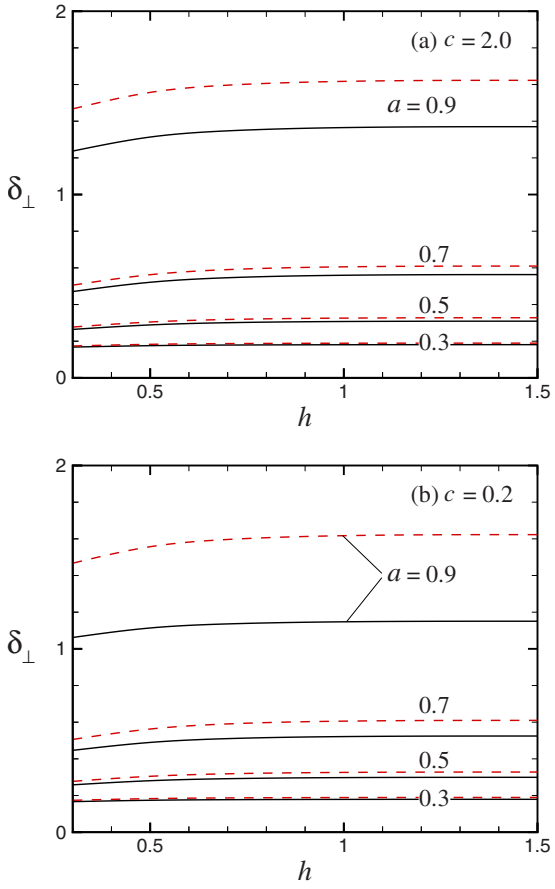

FIG. 8. (Color online) Transverse slip length $\delta_\perp$ as a function of the channel height h and gas area fraction of the wall a, where $\lambda=0.1$, $\mu=0.01$, and (a) $c=2$, (b) $c=0.2$. The dashes are for ideal gas $\mu=0$.

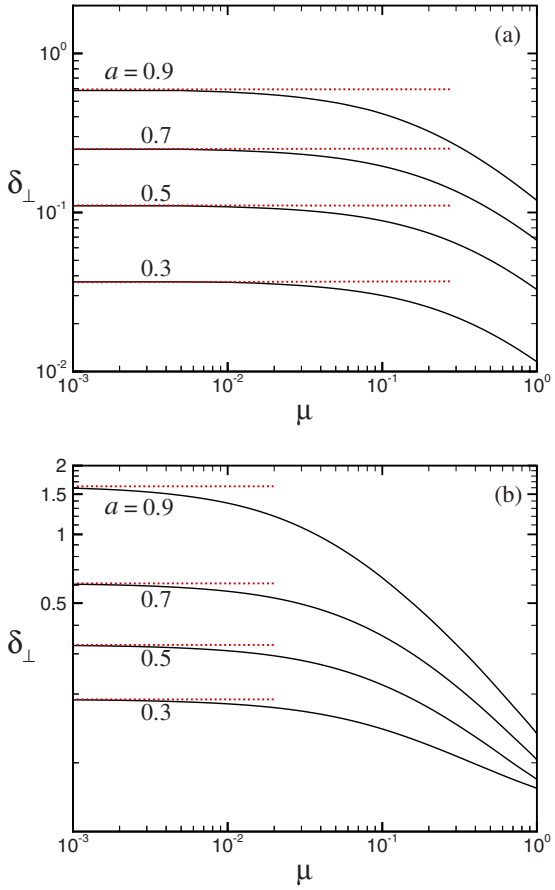

FIG. 9. (Color online) Transverse slip length $\delta_\perp$ as a function of the viscosity ratio μ and gas area fraction of the wall a, where $h=5$, $c=2$, and (a) $\lambda=0$, (b) $\lambda=0.1$. The dotted lines are the limits for ideal gas $\mu=0$.

encounters comparable friction over the two phases, despite a practically very small gas viscosity and a small degree of intrinsic slippage over the solid phase.

C. Phenomenological relations

Some researchers show favor to the development of simple and handy relationships based on the modeling predictions. These relationships do not necessarily have a physical basis, and in practice, are either heuristically derived or based on data-fitting. Maynes *et al.*[11] and Ybert *et al.*[7] put forward such phenomenological relationships to describe the effect of viscous dissipation in the gas phase on the slip length. The formula presented by Maynes *et al.*[11] is simply the no-shear model formula (17) modified by a factor that is a function of the cavity and channel dimensions. In terms of the present notation, their formula reads as follows:

$$\delta_\parallel^{(\mathrm{pred})} = \delta_{\parallel ZS}^{\mathrm{plate}}\left[1-\exp\left(-\frac{2^{5/3}c^{2/3}h^{1/3}}{a}\right)\right]. \tag{38}$$

This formula has been shown by Maynes *et al.*[11] to correlate very well with their simulation results for the following ranges of cavity dimensions: $0<a<0.969$, $0.1<1/2h<1$, and $0<c/4h<0.7$. Their formula, however, does not incorporate the gas/liquid viscosity ratio and the intrinsic slippage as controlling parameters.

For shear flow over a flat surface patterned with no-shear and no-slip regions, Ybert *et al.*[7] proposed an interpolation formula for an effective slip length accounting for the finite dissipation in the gas phase: $\delta_{\mathrm{eff}}^{-1}=\delta_g^{-1}+\delta_{ZS}^{-1}$, where δ_g is a local slip length (which is large, but not infinite) on the liquid-gas interface. As discussed earlier, the reciprocal δ_g^{-1} represents surface friction of the interface. Assuming Darcy–Brinkman flow in the gas phase, Ybert *et al.*[7] further derived an expression for δ_g in terms of the gas layer thickness, viscosity ratio, and solid fraction. Their expression, however, contains a parameter that depends on the microstructure housing the gas phase and cannot be determined theoretically in general.

Shown in Fig. 11(a) is a comparison between our modeling results $\delta_\parallel^{(\mathrm{mod})}$ and the predictions $\delta_\parallel^{(\mathrm{pred})}$ using the relationship (38) proposed by Maynes *et al.*[11] The symbols in this plot denote groups of inputs of $\lambda=0,0.05,0.1$ and $\mu=0.01,0.02$. Each group contains data points for $a=0.9,0.5$, $h=0.5,5$, $c=0.2,2$, which are within the above-mentioned ranges of dimensions explored by Maynes *et al.*[11] The groups with $a=0.5$ are those data points lying near the lower left corner of the graph. As expected, formula (38) predicts well only for those with zero intrinsic slippage, as this is the original setting in which it was proposed.

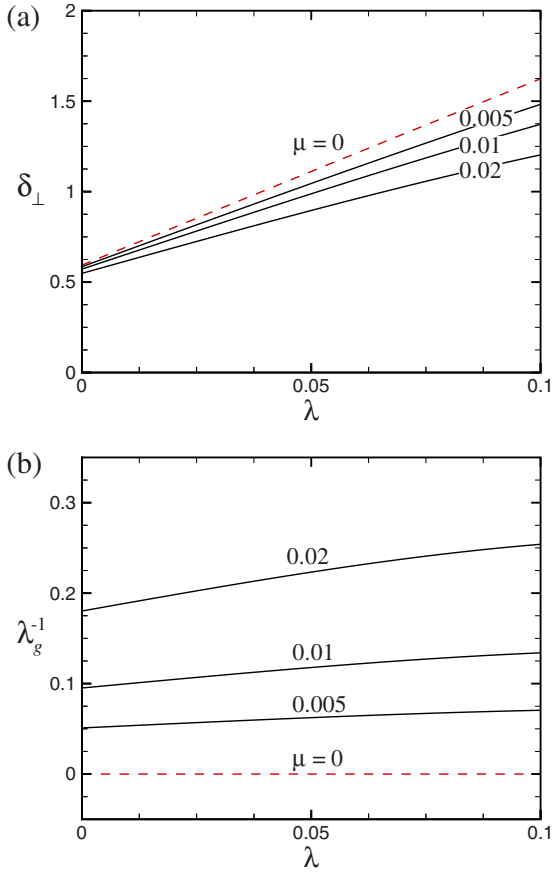

FIG. 10. (Color online) For $a=0.9$, $h=5$, and $c=2$, (a) transverse slip length $\delta_\perp$ as a function of the intrinsic slip length λ, for $\mu=0$, 0.005, 0.01, and 0.02, where the dotted lines are the values computed by the approximation formula (36); (b) reciprocal of the gas slip length λ_g^{-1} as a function of the intrinsic slip length λ, for $\mu=0$, 0.005, 0.01, and 0.02.

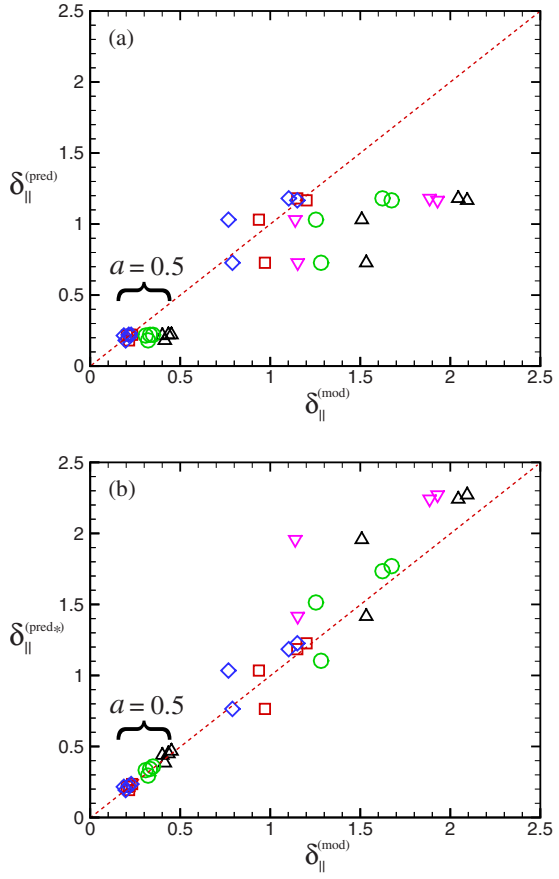

FIG. 11. (Color online) Comparison between the modeling values of effective slip length, $\delta_\parallel^{(mod)}$, and the predictions (a) $\delta_\parallel^{(pred)}$ using the formula (38), (b) $\delta_\parallel^{(pred*)}$ using the formula (39). The symbols denote the following groups: (i) squares for $\lambda=0$ and $\mu=0.01$, (ii) diamonds for $\lambda=0$ and $\mu=0.02$, (iii) circles for $\lambda=0.05$ and $\mu=0.01$, (iv) triangles for $\lambda=0.1$ and $\mu=0.01$, and (v) inverted triangles for $\lambda=0.1$ and $\mu=0.02$. Each group contains the following cases: $a=0.9,0.5$, $h=0.5,5$, $c=0.2,2$. The data points lying near the lower left corner of the graphs are those cases with $a=0.5$, while the others are those with $a=0.9$.

With modest intrinsic slippage $\lambda=0.05,0.1$, the formula predictions can be far off the modeling values, especially for $a=0.9$.

A simple way to improve the performance of the formula is to replace the no-shear slip length used in the formula. In Eq. (38), $\delta_{\parallel ZS}^{\text{plate}}$ is Philip's[14] expression for slip flow over a flat plate and is applicable to $\mu=0$, $\lambda=0$, and $h\gg 1$. Let us replace it by $\delta_{\parallel ZS}^{\text{channel}}$, which is the slip length for flow through a finite channel, where $\mu=0$, $\lambda>0$, and $h\geq O(1)$. This is the value that we have computed using the method of point collocation as described earlier. The modified formula is, therefore,

$$\delta_\parallel^{(\text{pred}*)} = \delta_{\parallel ZS}^{\text{channel}}\left[1-\exp\left(-\frac{2^{5/3}c^{2/3}h^{1/3}}{a}\right)\right]. \tag{39}$$

Figure 11(b) shows how the predictions using this modified formula are compared with the modeling values. Obviously, the overall agreement is much better than that shown in Fig. 11(a). The correlation is particularly good for the groups with $a=0.5$. For the groups with $a=0.9$, the correlation is also reasonably good, except for a few cases of fairly large deviations. On identifying the cases which are predicted well, we may infer from this comparison that relationship (39) can be applied with good confidence (within 20%) as long as $a\leq 0.9$, $\mu=O(0.01)$, $c>1$, $h=O(1)$, $\lambda\leq O(0.1)$. It would be desirable if the formula could be further developed incorporating the viscosity ratio and intrinsic slip length as two additional controlling parameters. Such an effort is, however, not pursued here.

We remark that, since there can be so many degrees of freedom in choosing curve-fitted parameters, a data-fitting formula with a wide scope of applicability is hard to come by in general. We further caution that any such deduced phenomenological formulas can only be used with great care; they generate estimates that can only be trusted for an accuracy within a factor of 2 or so. They are also good at, within the regimes of applicability, revealing the qualitative dependence of the slip lengths on the controlling parameters. They are of use if one is merely interested to do a rough calculation. If the intention is to get accurate predictions, the full models should always be used.

Nevertheless, for the sake of quick reference, let us summarize in Table I the key values that can be gathered from the present study. Based on our modeling results, we may compile some approximate figures representing the effect of a gas viscosity (relative to that of liquid) of 0.01 on the effective slip lengths when compared with those based on an

TABLE I. Approximate values representing the deviation of the effective longitudinal and transverse slip lengths $(\delta_{\parallel}, \delta_{\perp})$ based on gas viscosity $\mu=0.01$ from the corresponding values $(\delta_{\parallel ZS}, \delta_{\perp ZS})$ based on ideal inviscid gas for $a=0.9-0.5$ and $h \geq O(1)$. The upper and lower limits are for $a=0.9$ and $a=0.5$, respectively. The values can be extended to other values of μ by linear interpolation as long as $\mu \leq O(0.01)$. Recall that all length dimensions are normalized by half the pitch of the wall micropattern.

Percentage decrease in the effective slip lengths	Longitudinal $(\delta_{\parallel ZS}-\delta_{\parallel})/\delta_{\parallel ZS}$		Transverse $(\delta_{\perp ZS}-\delta_{\perp})/\delta_{\perp ZS}$	
Intrinsic slip length	$\lambda=0$	$\lambda=0.1$	$\lambda=0$	$\lambda=0.1$
Shallow cavity $c \sim 0.2$ (%)	20–10	30–10	10–5	30–10
Deep cavity $c \geq 2$ (%)	3–1	10–3	4–2	15–6

ideal inviscid gas under the conditions that have been investigated. The upper and lower limits of the values in the table are for $a=0.9$ and $a=0.5$, respectively. It is expected that if a exceeds 0.9 and gets closer to unity, the values can be several times higher than the upper limits given here. Also, these values need to be adjusted (approximately linearly) if the gas viscosity μ varies mildly about 0.01 (i.e., a multiplying factor of 2 if $\mu=0.02$, and so on) After all, the values presented in Table I are only intended for a quick but approximate estimation of the effect of gas viscosity on the effective slip lengths for Stokes flow through a channel with superhydrophobic grooved walls.

One can see from Table I that the gas viscosity is to have different degrees of influence on the longitudinal and transverse slip lengths. A ratio of these two slip lengths is important to flow through a microchannel containing superhydrophobic surface with inclined grooves.[6,12] Anisotropy arises from the fact that $\delta_{\perp}$ is always smaller than $\delta_{\parallel}$ and flow can be induced both in a direction along and normal to the applied pressure gradient. We show in Fig. 12 how the cavity depth and the intrinsic slip length may affect the effective slip length ratio. For a deep cavity, the gas viscous dissipation is to decrease $\delta_{\perp}$ more than $\delta_{\parallel}$, and hence the ratio $\delta_{\perp}/\delta_{\parallel}$ is smaller than the one for gas with zero viscosity. The opposite is true for a shallow cavity, for which $\delta_{\perp}$ is less decreased than $\delta_{\parallel}$ by the gas viscous effect.

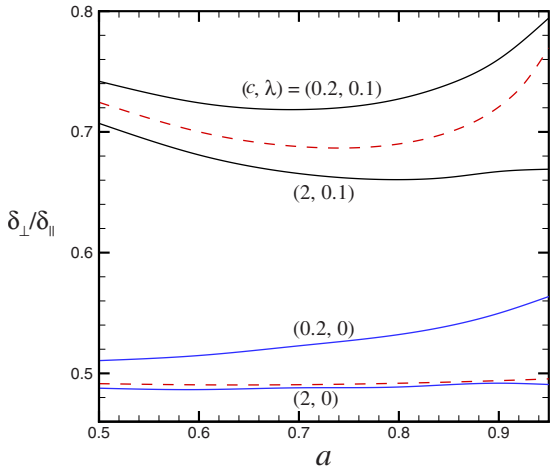

FIG. 12. (Color online) Ratio of the effective transverse to longitudinal slip lengths, $\delta_{\perp}/\delta_{\parallel}$, as a function of the gas area fraction of the wall, a, for $\mu=0.01$, $h=1$, $c=0.2, 2$, and $\lambda=0, 0.1$. The dashes are for ideal gas $\mu=0$.

IV. CONCLUDING REMARKS

We have developed a computationally efficient liquid-gas coupled model to simulate Stokes flow of a liquid through a microchannel whose walls are micropatterned with longitudinal or transverse grooves filled with a gas. We have found that under the combination of the following conditions even a small gas/liquid viscosity ratio may lead to appreciable effects on the macroscopic slip lengths. First, a sufficiently large gas area fraction of the wall $(a>0.5)$. Second, sufficiently shallow grooves $(c<0.5)$. Third, with intrinsic slippage of the solid phase $(\lambda>0)$. We have also found that, under the second or the third condition, the slip lengths can be sensitively affected by a viscosity ratio as small as $O(0.01)$. This has been explained by looking into the surface friction of the liquid-gas interface, which may increase quickly with the viscosity ratio.

Based on the modeling results, we have presented values in Table I that can be used for quick but approximate estimates of the slip lengths as functions of the cavity dimensions and other parameters. The results presented in this paper will help one to estimate the validity of assuming zero-gas viscosity on the mathematical modeling of slip flow over a micropatterned surface.

Meniscus curvature or liquid penetration into grooves, which are ignored in this study, will further affect the slip lengths. In addition, when the pattern is in an out-of-phase arrangement on the two walls, the results can be qualitatively changed, depending on the pattern being longitudinal or transverse, for flow through a thin channel. It is worthwhile if a more comprehensive model taking into account all these effects can be developed.

ACKNOWLEDGMENTS

The work was supported by the Research Grants Council of the Hong Kong Special Administrative Region, China, through Project No. HKU 715609E, and also by the University of Hong Kong through the Small Project Funding Scheme under Project Code No. 200807176081, and the Seed Funding Programme for Basic Research under Project Code No. 200911159024.

[1] C. Neto, D. R. Evans, E. Bonaccurso, H. J. Butt, and V. S. J. Craig, "Boundary slip in Newtonian liquids: A review of experimental studies," Rep. Prog. Phys. **68**, 2859 (2005).
[2] E. Lauga, M. P. Brenner, and H. A. Stone, in *Handbook of Experimental Fluid Dynamics* (Springer, New York, 2007), Chap. 19, pp. 1219–1240.
[3] X. Zhang, F. Shi, J. Niu, Y. Jiang, and Z. Wang, "Superhydrophobic sur-

faces: From structural control to functional application," J. Mater. Chem. **18**, 621 (2008).
[4]J. P. Rothstein, "Slip on superhydrophobic surfaces," Annu. Rev. Fluid Mech. **42**, 89 (2010).
[5]C. L. M. H. Navier, "Memoire sur les lois du movement des fluids," Memoires de l'Academie Royale des Sciences de l'Institut de France **6**, 389 (1823).
[6]C. J. Teo and B. C. Khoo, "Analysis of Stokes flow in microchannels with superhydrophobic surfaces containing a periodic array of micro-grooves," Microfluid. Nanofluid. **7**, 353 (2009).
[7]C. Ybert, C. Barentin, and C. Cottin-Bizonne, "Achieving large slip with superhydrophobic surfaces: Scaling laws for generic geometries," Phys. Fluids **19**, 123601 (2007).
[8]Y. P. Cheng, C. J. Teo, and B. C. Khoo, "Microchannel flows with superhydrophobic surfaces: Effects of Reynolds number and pattern width to channel height ratio," Phys. Fluids **21**, 122004 (2009).
[9]C. J. Teo and B. C. Khoo, "Flow past superhydrophobic surfaces containing longitudinal grooves: Effects of interface curvature," Microfluid. Nanofluid. **9**, 499 (2010).
[10]J. Davies, D. Maynes, B. W. Webb, and B. Woolford, "Laminar flow in a microchannel with superhydrophobic walls exhibiting transverse ribs," Phys. Fluids **18**, 087110 (2006).
[11]D. Maynes, K. Jeffs, B. Woolford, and B. W. Webb, "Laminar flow in a microchannel with hydrophobic surface patterned microribs oriented parallel to the flow direction," Phys. Fluids **19**, 093603 (2007).
[12]C. Y. Wang, "Flow over a surface with parallel grooves," Phys. Fluids **15**, 1114 (2003).
[13]C. O. Ng and C. Y. Wang, "Stokes shear flow over a grating: Implications for superhydrophobic slip," Phys. Fluids **21**, 013602 (2009).
[14]J. R. Philip, "Flows satisfying mixed no-slip and no-shear conditions," Z. Angew. Math. Phys. **23**, 353 (1972).
[15]C. Cottin-Bizonne, C. Barentin, E. Charlaix, L. Bocquet, and J.-L. Barrat, "Dynamics of simple liquids at heterogeneous surface: Molecular-dynamics simulations and hydrodynamic description," Eur. Phys. J. E **15**, 427 (2004).
[16]S. C. Hendy and N. J. Lund, "Effective slip boundary conditions for flows over nanoscale chemical heterogeneities," Phys. Rev. E **76**, 066313 (2007).